

Graphene on Si(111)7×7

O Ochedowski¹, G Begall¹, N Scheuschner², M El Kharrazi¹,
J Maultzsch² and M Schleberger¹

¹ Fakultät für Physik and CeNIDE, Universität Duisburg-Essen, D-47048 Duisburg, Germany

² Institut für Festkörperphysik, Technische Universität Berlin, D-10623 Berlin, Germany

E-mail: marika.schleberger@uni-due.de

Received 4 June 2012, in final form 20 August 2012

Published 21 September 2012

Online at stacks.iop.org/Nano/23/405708

Abstract

We demonstrate that it is possible to mechanically exfoliate graphene under ultrahigh vacuum conditions on the atomically well defined surface of single crystalline silicon. The flakes are several hundred nanometers in lateral size and their optical contrast is very faint, in agreement with calculated data. Single-layer graphene is investigated by Raman mapping. The graphene and 2D peaks are shifted and narrowed compared to undoped graphene. With spatially resolved Kelvin probe measurements we show that this is due to p-type doping with hole densities of $n_h \simeq 6 \times 10^{12} \text{ cm}^{-2}$. The *in vacuo* preparation technique presented here should open up new possibilities to influence the properties of graphene by introducing adsorbates in a controlled way.


(Some figures may appear in colour only in the online journal)

1. Introduction

Graphene with its unique electronic properties is often envisaged as the material for future field effect transistors and other electronic devices [1]. Up to now graphene of the best quality with respect to important parameters such as e.g. charge carrier mobility has been obtained by mechanical exfoliation [2–4]. This method makes use of adhesive tape and is applied under ambient conditions. It is therefore not surprising that usually graphene flakes as well as devices are heavily contaminated by residual glue, adsorbates such as water, carbohydrates and photoresist residues [5–7]. This is a major drawback in comparison with the ultraclean epitaxial graphene flakes grown on SiC for example [8, 9]. Ishigami *et al* have proposed a method for *in situ* cleaning of photolithographically processed devices which involves annealing in H₂ at 400 °C [10], but the devices are frequently operated under ambient conditions, again introducing contaminants. It has been shown already that these contaminants significantly influence the properties of graphene, as they may act as electron acceptors or donors [11–13]. Charged impurities shift the Fermi level, may

cause scattering by Coulomb interaction and may also be the origin of electron–hole puddles [14]. It is therefore very important to be able to investigate the specific influence of the respective adsorbates on graphene to better understand variations in transport properties of gated devices and to develop appropriate methods for their improvement. But due to the rather arbitrary nature of the contaminants this has remained impossible until now.

In this paper we show that graphene flakes can be exfoliated directly on a crystalline Si surface (without an oxide layer) under the cleanest conditions possible, allowing access to unprecedented information. In addition, it has just recently been demonstrated that graphene/silicon hybrid structures are a very promising candidate for future transistors, due to the adjustable Schottky barrier between the two materials [15]. The preparation procedure used in this work is based on the adhesion or cohesion of two solids by attractive forces without any glue. This technique is widely used in microelectronics [16], called fusion bonding or wafer direct bonding. The idea goes back to Rayleigh, who investigated the adhesion of polished fused quartz samples [17]. The phenomenon occurs only with nearly perfectly flat and clean surfaces. The exact nature of the bonding depends crucially on the surface cleanliness. Under ambient conditions, water adlayers, carbohydrates or other surface species are present and the attractive forces are mainly

 Content from this work may be used under the terms of the [Creative Commons Attribution-NonCommercial-ShareAlike 3.0 licence](http://creativecommons.org/licenses/by-nc-sa/3.0/). Any further distribution of this work must maintain attribution to the author(s) and the title of the work, journal citation and DOI.

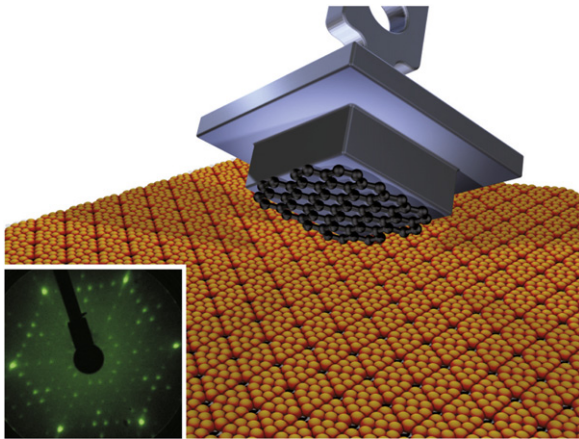


Figure 1. Schematic of the stamping procedure. The graphite flake is attached to a metal stamp which can be brought into contact with the Si(111)7×7 surface by means of a wobble stick. Inset: typical LEED image of the 7×7 reconstruction acquired after thermal processing; electron energy $E = 50$ eV.

van der Waals or hydrogen bonds. The bonding type can be changed to covalent bonds and thus strengthened by thermal processing. In the extreme case of ultraclean surfaces in ultrahigh vacuum (UHV), however, covalent bonds can form directly even at room temperature [18].

2. Experimental details

As a substrate we use a silicon wafer (n-doped, 10–20 Ω cm, Crystec) with the surface oriented perpendicular to the [111]-direction. The Si sample is introduced into an UHV chamber at a base pressure of $p_b \leq 1 \times 10^{-10}$ mbar and degassed at $T = 650$ °C for 24 h. The Si is then repeatedly flash-heated up to $T = 1250$ °C for a few seconds by direct current heating. During flashing the pressure remains below $p = 5 \times 10^{-9}$ mbar. This procedure completely removes the native oxide layer from the Si surface and results in the equilibrium structure of Si(111), the well known 7×7-reconstruction [19], upon cooling down through the transition temperature of 850°. The successful preparation is controlled by low-energy electron diffraction (LEED, OCI BDL800IR microchannel plate version). This method allows for a quick and direct determination of the surface periodicity. Sharp spots and a low background intensity indicate that the surface is well ordered. The typical pattern shown in the inset of figure 1 only appears if the silicon oxide layer has been successfully removed and the clean Si(111) surface has reconstructed into its minimum energy state. After the Si(111)7×7 surface has been prepared and cooled down again to RT, a freshly cleaved crystal of highly oriented pyrolytic graphite (HOPG), which has previously been degassed at $T = 120$ °C for 24 h, is gently pressed onto the Si surface by means of a wobblestick, as schematically shown in figure 1. The Si sample with exfoliated graphene is then removed from the vacuum chamber for further inspection. *Ex situ* optical inspection and atomic force microscopy (AFM, Veeco Dimension 3100) reveal that the stamping leads to randomly

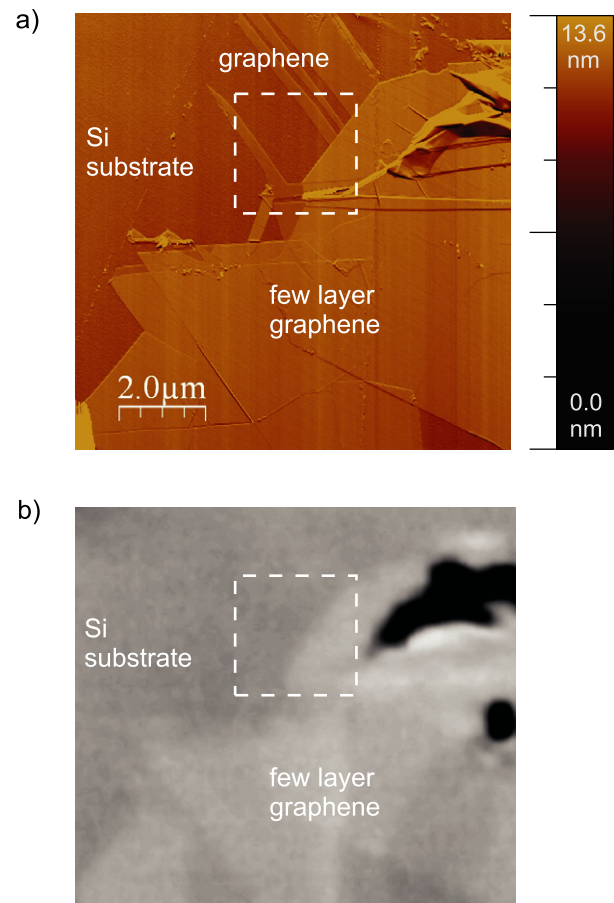


Figure 2. (a) Atomic force microscopy (tapping mode, nanosensors NCHR with $f = 290$ kHz; scan frequency 0.8 Hz) images of graphene exfoliated under UHV conditions. The dashed rectangle marks the region shown in more detail in figure 5. The graphite regions can be used to calibrate Kelvin probe data (see text). (b) Optical microscopy image of the same region as in (a). The optical contrast is very feeble and prevents easy identification of single-layer graphene.

distributed flakes of graphite on the surface, among which also graphene can be found, see figure 2. Note that the extraction of the sample was done here only to simplify the measurements, because UHV setups can be equipped to perform AFM and Kelvin probe measurements [20], but are usually not compatible with optical inspection and μ -Raman mapping. Nevertheless, as we have proved the feasibility of the deposition technique, future experiments can be easily performed totally *in situ*.

3. Results and discussion

With respect to graphene it was discussed earlier already that *in situ* stamping of graphene should in principle be feasible on crystalline SiO₂ [21]. The authors calculated the energy of adhesion and cohesion, respectively, using a density functional approach. It was found that the cleavage of graphite in contact with a completely oxygen-terminated SiO₂ surface is very likely, as it is energetically favorable. However, the experiment was performed under ambient conditions and they

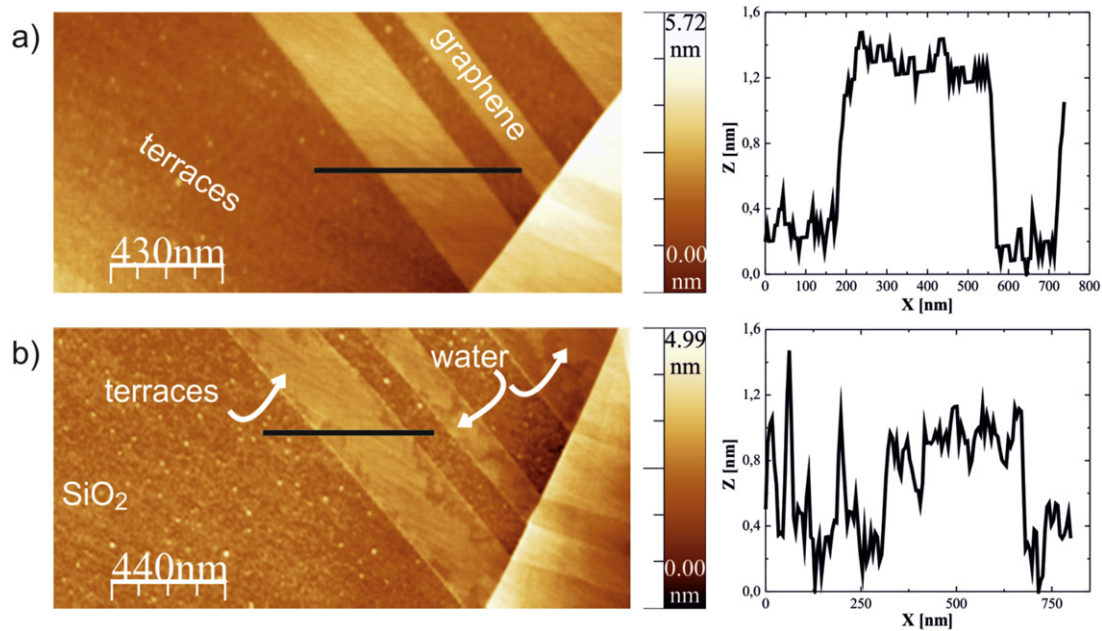


Figure 3. AFM images and corresponding line scans of a substrate region covered with single-layer graphene, i.e. inside the marked region of figure 2. (a) Image taken shortly after extraction from the UHV and before Raman mapping. The original terrace morphology of the Si substrate shows signs of a beginning oxidation, the steps are preserved underneath graphene. SLG height appears to be ≈ 1 nm. (b) Image taken after Raman mapping which has induced water adlayers. The uncovered Si(111) substrate is fully oxidized and the original terrace structure has completely disappeared. Underneath graphene terraces can still be recognized. SLG height is now 0.4–0.6 nm (see text).

did not obtain single-layer (SLG) but only few-layer graphene (FLG). The cohesion energy of Si is typically large ($\gamma > 2 \text{ J m}^{-2}$) [18] and comparable to SiO_2 , thus one could argue along this line that the chance for SLG production should be reasonable in our case. With our approach contamination by ambient conditions is avoided and both surfaces are very flat, thus approaching ideal conditions for fusion bonding. In addition, the Si(111) 7×7 surface is known to be extremely reactive due to its specific reconstruction with unterminated bonds at the adatom positions, i.e. with a density of one dangling bond per 5 \AA^2 . This effect could increase the probability of covalent bond formation and may thus play an even bigger role here.

Chen *et al* used a cleaned and passivated Si surface and exfoliation in air to create a silicon/graphene device with a Schottky barrier [22]. The ideality factor of their devices was, however, much lower than the one achieved with the method presented in [15], indicating that the interface quality is much worse despite the clean Si surface. Ritter *et al* have applied the so-called dry contact transfer method, where a braided fiberglass applicator is loaded with powder of exfoliated graphite [23]. The applicator can be heated in UHV so that physisorbed contamination is removed. Subsequently, the applicator is brought into contact with the substrate. This procedure yields a high percentage of single-layer graphene. However, the lateral dimensions of the resulting flakes is around 20 nm. Therefore, this approach produces flakes which are much too small to be investigated by means of Raman spectroscopy, and they are not suitable for device fabrication.

This is different from the technique presented here. Typical images from stamped graphene on Si(111) 7×7

taken with an optical microscope are shown in figure 2(b). The flake distribution and size resembles the one typically found with exfoliation under ambient conditions on various substrates [24]. The lateral size is in principle limited by the quality of the HOPG crystal, but additional preparation steps may also be needed to obtain larger flakes. Graphene flakes appear brighter than the substrate, but the contrast is very faint, i.e. $C \approx -10 \pm 7\%$ for 7 layers, $C \approx -6 \pm 6\%$ for 4 layers, and $C \leq -1\%$ for SLG. To correlate the contrast values from the optical image with the number of graphene layers, Raman and AFM measurements were analyzed in the corresponding areas. These values have the correct sign, i.e. flakes appear brighter than the substrate, and are somewhat higher than the calculated data using a Fresnel law based model [25].

From our AFM data (see figures 3 and 5) we find a minimum average height of graphene of ≤ 1 nm, which would be in good agreement with either single-layer or bilayer graphene, assuming an interlayer spacing of graphite of 3.5 \AA . We also find layers with 2 and 3 nm height with respect to the substrate. It is very well known that height measurements of graphene with tapping mode AFM are not unambiguous [26]. Here, the post-oxidization of the Si(111) surface causes an additional uncertainty.

Due to the exposure to ambient conditions at least the parts of the substrate without graphene are covered by a native oxide layer of $d_{\text{SiO}_2} \approx 1.5$ nm thickness after several hours. It has recently been shown that graphene protects the underlying surface quite well even to the extreme of preserving the very sensitive surface state of Ir(111) under ambient conditions [27]. Therefore, the clean non-oxidized

Si surface and even the 7×7 -reconstruction might still be present underneath the graphene layer. Samples with SLG freshly taken out from the UHV show no signs of water or adsorbates for some hours, see figures 3(a) and 5. We took great care to measure Kelvin probe and Raman point spectra with the sample in this condition. This is important, because a significant contamination with water is introduced by the prolonged laser irradiation from the Raman mapping, as can be seen from the direct comparison before/after in figures 3(a) and (b), see also [28]. Note, that despite the presence of the Raman-induced water adlayer the original terrace steps under the graphene sheet are still visible, indicating that in contrast to the exposed Si(111) surface, no oxidation has taken place in areas protected by graphene. An additional indication for the protection properties comes from a more detailed analysis of the AFM images. The line profile of the pristine SLG shows a height of about 1 nm with respect to the SiO₂ surface, see figure 3. After the Raman mapping, water is present on the sample but it is not completely covered, as can be clearly seen in figure 3(b). The SLG with the water adlayer exhibits a different height profile: 0.6 nm in areas where water is present and 0.4 nm in areas where there is no water, see line scans in figure 3. The difference in height of 0.4 nm (exposed to ambient conditions, figure 3(a)) instead of ≈ 1.0 nm (pristine, figure 3(b)) is consistent with the assumption that the oxide layers has grown while the Si(111) underneath the graphene has been protected from oxidation. This again is consistent with the recently published findings that even graphene deposited by chemical vapor deposition is able to protect metallic substrates such as Cu and Cu/Ni alloy from oxidation [29].

To check whether optical data can support this observation we have calculated the optical contrast $C = \frac{R_0 - R}{R_0}$, with R the reflected intensity with and R_0 the reflected intensity without graphene. We assumed full oxidation underneath the graphene layer (model 1) and complete protection by graphene (model 2), respectively. From figure 4 one can see that the absolute contrast values are in general higher for model 2. However, even under the most favorable conditions, e.g. blue light and at least 14 layers of graphene, the maximum contrast difference for the two models would be $\Delta C = C_{\text{model 1}} - C_{\text{model 2}} = 1.3\%$, which is clearly beyond our experimental resolution. This means that the contrast differences we observe in figure 4 are not sufficient to differentiate between an oxidized and non-oxidized Si surface.

We used μ -Raman spectroscopy (LabRAM HR, Horiba Jobin Yvon) with an excitation wavelength of $\lambda = 532$ nm to verify and investigate the SLG. The incident power was kept below 5 mW to prevent heating. As already discussed, we still observed the formation of water adlayers after the Raman mapping, while short point spectra did not show any effect. The spectra were calibrated with neon lines. We performed a Raman mapping with a step size of 250 nm and a laser spot of < 0.5 μm diameter. To extract the Raman shift, intensity and a full width at half maximum (FWHM) from the data, the G mode and the 2D mode were fitted separately with a single Lorentzian. From the resulting FWHM map of the 2D

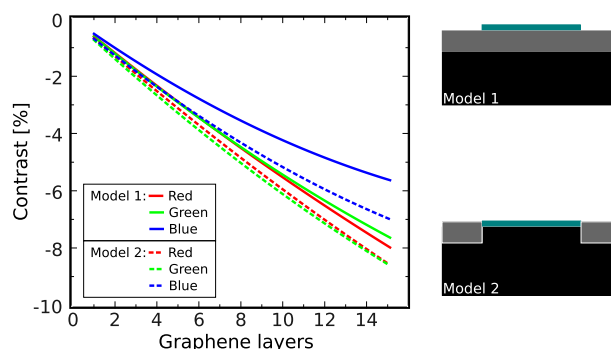


Figure 4. Calculated contrast values C in per cent for varying numbers of graphene layers and different color channels using the Fresnel law [25]. Model 1, solid lines: complete oxidation of Si underneath graphene. Model 2, dashed lines: complete protection from oxidation of Si by graphene.

mode (see figure 6(a)) we identify an SLG region (indicated by the rectangle) as well as surrounding few-layer graphene and graphite. Figure 6(c) shows Raman spectra from the SLG as well as from the FLG region. The 2D mode for the SLG is found at 2673 cm^{-1} , with a FWHM of 27 cm^{-1} , and exhibits the narrow symmetric line shape characteristic for SLG [30]. The absence of the disorder-induced D peak at 1350 cm^{-1} indicates high structural integrity of the flakes, which is typical for exfoliated graphene.

In the SLG region the G mode is upshifted up to 1593 cm^{-1} and strongly narrowed (FWHM 7 cm^{-1}) compared to undoped graphene, which shows a Raman shift of 1583 cm^{-1} with a FWHM of 15 cm^{-1} [31]. This is clear evidence of doping, with an estimated carrier concentration of $n \geq 4 \times 10^{12}$ cm^{-2} [31–33]. In the few-layer graphene regions (see figure 6(b)) the G mode shows lower frequencies, indicating less effective doping in thicker layers. However, for an accurate quantification of type and value of the charge carrier concentration one would have to perform experiments with a defined gate structure.

To study the doping of graphene we measured the locally resolved contact potential difference (LCPD) between the tip and the sample with a Kelvin probe setup [34]. Kelvin probe measurements were performed before the Raman mapping to avoid water contamination. Images were recorded in a two-pass mode. During the first pass the topography is measured in tapping mode and during the second pass the tip is lifted by 3–10 nm. While lifted, an ac bias of about $U_{\text{Bias}} = 0.5$ – 1.0 V is applied to the tip at its resonance frequency. The resulting electric force on the tip is minimized with a dc voltage that corresponds to the LCPD between the tip and the measured area [35]. From figures 5(b) and (c), one can clearly see that the LCPD is decreasing with decreasing layer thickness. We attribute this to a p-type doping of graphene [36, 37, 20].

Attributing the known work function of $\Phi_{\text{HOPG}} = 4.65$ eV (see [38] and references therein) to the CPD value of the graphite regions enables us to assign work function values to our graphene layers: $\Phi_{G_i} = \Phi_{\text{HOPG}} + \Delta\text{CPD}(\text{FLG} - G_i)$, i being the number of graphene layers. To exclude any ambiguities the number of layers was determined by the

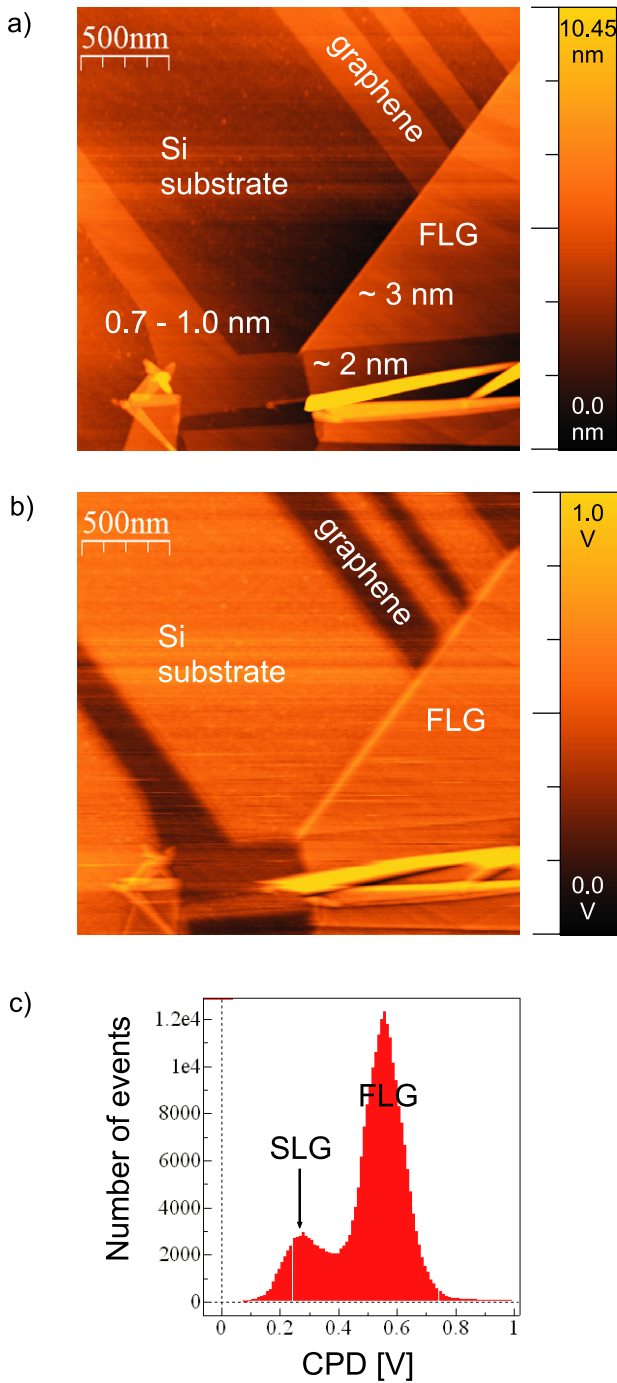


Figure 5. (a) AFM image of region marked in figure 2 where typical heights of SLG and FLG with respect to the substrate can be seen. (b) LCPD image of SLG and substrate as well as FLG (region marked in figure 2) obtained by Kelvin probe microscopy. A bias voltage was applied to the tip. Single-layer graphene was verified by Raman spectroscopy. (c) CPD histogram from (b).

shape of the 2D Raman peak for SLG and TLG, and only thicker layers were determined by AFM line scans, assuming a height of 0.35 nm for each layer. We can thus determine the absolute value of the work function of SLG to be $\Phi = 4.93 \pm 0.1$ eV (see figure 7). For SLG, the work function variation due to doping corresponds to a shift of the Fermi energy ΔE_F with respect to the Dirac point [37]. The upshift

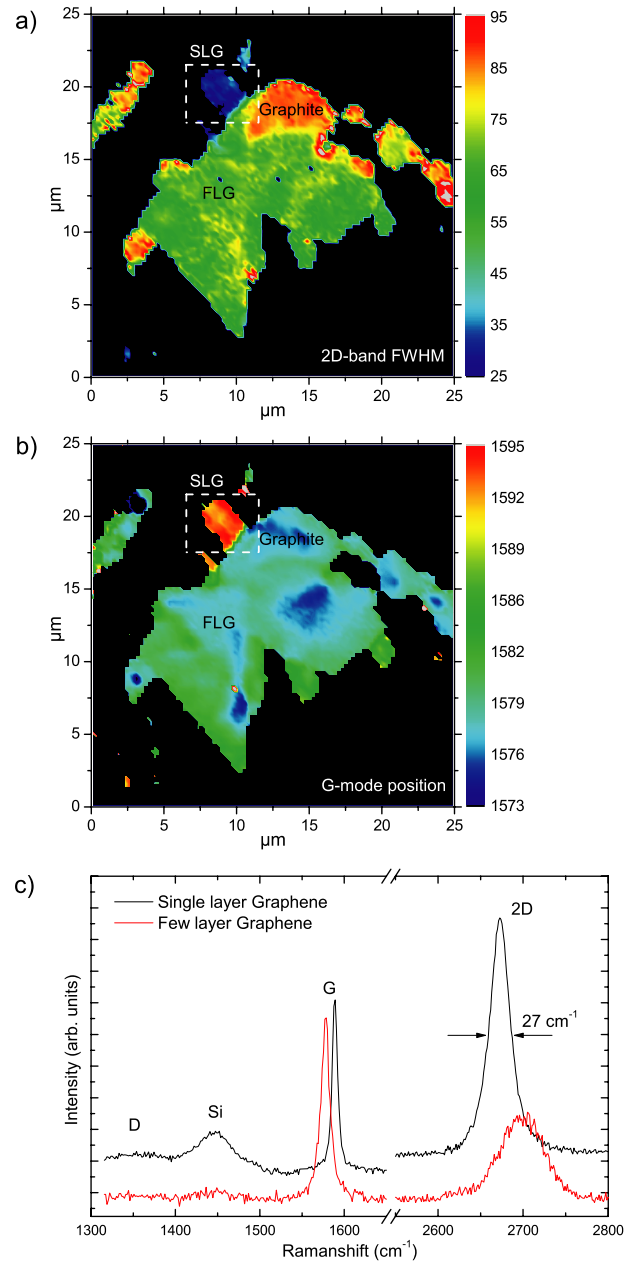


Figure 6. (a) Raman 2D FWHM map of the sample region shown in figure 2. (b) Raman G mode map of the sample region shown in figure 2. (c) Shape and width of the Raman 2D mode at 2675 cm^{-1} are characteristic for single-layer graphene. Shift and narrowing of the G mode indicate doping.

of the Fermi level with respect to the value for undoped free-standing graphene, $\Phi = 4.57\text{--}4.7$ eV [39–41], is $\Delta E_F \approx 290$ meV. This corresponds to a charge carrier density of $n_h = \frac{1}{\pi} \left(\frac{\Delta E_F}{\hbar v_F} \right)^2 \approx 6 \times 10^{12} \text{ cm}^{-2}$ if we assume $v_F = 1 \times 10^6 \text{ m s}^{-1}$ for the Fermi velocity [42]. These numbers have to be treated with great care, as the exposure to ambient conditions might influence the work function of HOPG and the calculated doping level [43]. Note, however, that the number agrees rather well with the number obtained from the shift of the Raman G mode (see figure 6). Whether the accumulation of holes observed here is indeed due to the direct interaction

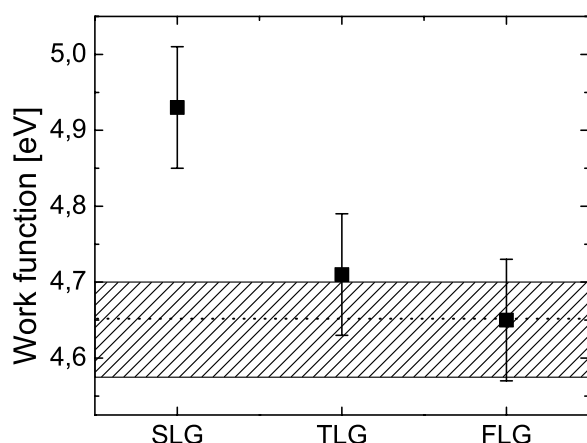


Figure 7. Work functions of single-, tri- and few-layer graphene on Si substrate determined from Kelvin probe measurements. The dashed line corresponds to the workfunction of HOPG, the hatched region corresponds to values given in the literature for free-standing (undoped) single-layer graphene.

of graphene with the clean silicon surface thus needs to be investigated in future experiments avoiding the exposure to ambient conditions altogether.

4. Conclusions

In summary, we have presented a method for the deposition of single-layer graphene flakes on Si(111)7×7 under UHV conditions. As the flakes reach lateral sizes of several hundred nanometers, this technique opens up a wide range of possible experiments, reaching from detailed studies of adsorbate doping and cleaning protocols to the development of more refined stamping procedures. The latter could include e.g. sputtered substrates, thermal processing steps or intercalated HOPG crystals to facilitate single-layer exfoliation. Our approach could also help to understand the origin of the strong differences in ideality factors in current graphene/silicon devices.

Acknowledgments

This work has been supported by the German Science Foundation (SPP 1459: Graphene and SFB 616: Energy dissipation at surfaces).

References

- [1] Kim K, Choi J-Y, Kim T, Cho S-H and Chung H-J 2011 A role for graphene in silicon-based semiconductor devices *Nature* **479** 338
- [2] Novoselov K S, Jiang D, Schedin F, Booth T J, Khotkevich V V, Morozov S V and Geim A K 2004 Two-dimensional atomic crystals *Proc. Natl Acad. Sci.* **102** 10451
- [3] Morozov S, Novoselov K, Katsnelson M, Schedin F, Elias D, Jaszczak J and Geim A 2008 Giant intrinsic carrier mobilities in graphene and its bilayer *Phys. Rev. Lett.* **100** 016602
- [4] Bolotin K I, Sikes K J, Jiang Z, Klima M, Fudenberg G, Hone J, Kim P and Stormer H L 2008 Ultrahigh electron mobility in suspended graphene *Solid State Commun.* **146** 351
- [5] Katsnelson M I 2010 Just add water *Science* **329** 1157
- [6] Cao P, Xu K, Varghese J O and Heath J R 2011 The microscopic structure of adsorbed water on hydrophobic surfaces under ambient conditions *Nano Lett.* **11** 5581
- [7] Lin Y-C, Lu C-C, Yeh C-H, Jin C, Suenaga K and Chiu P-W 2012 Graphene annealing: how clean can it be? *Nano Lett.* **12** 414
- [8] Berger C 2006 Electronic confinement and coherence in patterned epitaxial graphene *Science* **312** 1191
- [9] Emtsev K V, Speck F, Seyller Th and Ley L 2008 Interaction, growth, and ordering of epitaxial graphene on SiC{0001} surfaces: a comparative photoelectron spectroscopy study *Phys. Rev. B* **77** 155303
- [10] Ishigami M, Chen J H, Cullen W G, Fuhrer M S and Williams E D 2007 Atomic structure of graphene on SiO₂ *Nano Lett.* **7** 1643
- [11] Adam S, Hwang E H, Galitski V M and Das Sarma S 2007 A self-consistent theory for graphene transport *Proc. Natl Acad. Sci.* **104** 18392
- [12] Hwang E, Adam S and Sarma S 2007 Carrier transport in two-dimensional graphene layers *Phys. Rev. Lett.* **98** 186806
- [13] Moser J, Verdaguier A, Jimenez D, Barreiro A and Bachtold A 2008 The environment of graphene probed by electrostatic force microscopy *Appl. Phys. Lett.* **92** 123507
- [14] Ponomarenko L A, Yang R, Mohiuddin T M, Katsnelson M I, Novoselov K S, Morozov S V, Zhukov A A, Schedin F, Hill E W and Geim A K 2009 Effect of a high-k environment on charge carrier mobility in graphene *Phys. Rev. Lett.* **102** 206603
- [15] Yang H, Heo J, Park S, Song H J, Seo D H, Byun K-E, Kim P, Yoo I, Chung H-J and Kim K 2012 Graphene barristor, a triode device with a gate-controlled Schottky barrier *Science* **336** 1140
- [16] Christiansen S H, Singh R and Goesele U 2006 Wafer direct bonding: from advanced substrate engineering to future applications in micro/nanoelectronics *Proc. IEEE* **94** 2060
- [17] Strutt R J (Lord Rayleigh) 1936 A study of glass surfaces in optical contact *Proc. R. Soc. Ser. A* **156** 326
- [18] Gösele U, Stenzel H, Martini T, Steinkirchner J, Conrad D and Scheerschmidt K 1995 Self-propagating room-temperature silicon wafer bonding in ultrahigh vacuum *Appl. Phys. Lett.* **67** 3614
- [19] Takayanagi K, Tanishiro Y, Takahashi S and Takahashi M 1985 Structure analysis of Si(111)-7×7 reconstructed surface by transmission electron diffraction *Surf. Sci.* **164** 367
- [20] Bussmann B Kleine, Ochedowski O and Schleberger M 2011 Doping of graphene exfoliated on SrTiO₃ *Nanotechnology* **22** 265703
- [21] Li D, Windl W and Padture N P 2009 Toward site-specific stamping of graphene *Adv. Mater.* **21** 1243
- [22] Chen Ch-Ch, Aykol M, Chang Ch-Ch, Levi A F J and Cronin S B 2011 Graphene-silicon Schottky diodes *Nano Lett.* **11** 1863
- [23] Ritter K A and Lyding J W 2008 Characterization of nanometer-sized, mechanically exfoliated graphene on the H-passivated Si(100) surface using scanning tunneling microscopy *Nanotechnology* **19** 015704
- [24] Akcöltekin S, El Kharrazi M, Köhler B, Lorke A and Schleberger M 2009 Graphene on insulating crystalline substrates *Nanotechnology* **20** 155601
- [25] Blake P, Hill E W, Castro Neto A H, Novoselov K S, Jiang D, Yang R, Booth T J and Geim A K 2007 Making graphene visible *Appl. Phys. Lett.* **91** 063124

- [26] Nemesincze P, Osvath Z, Kamaras K and Biro L 2008 Anomalies in thickness measurements of graphene and few layer graphite crystals by tapping mode atomic force microscopy *Carbon* **46** 1435
- [27] Varykhalov A, Marchenko D, Scholz M R, Rienks E D L, Kim T K, Bihlmayer G, Sánchez-Barriga J and Rader O 2012 Ir(111) surface state with giant Rashba splitting persists under graphene in air *Phys. Rev. Lett.* **108** 066804
- [28] Ochedowski O, Kleine Bußmann B and Schleberger M 2012 Laser cleaning of exfoliated graphene *MRS Symp. Proc.* **1455** mrs12-1455-ii08-06
- [29] Chen S *et al* 2011 Oxidation resistance of graphene-coated Cu and Cu/Ni alloy *ACS Nano* **5** 1321
- [30] Ferrari A C *et al* 2006 Raman spectrum of graphene and graphene layers *Phys. Rev. Lett.* **97** 187401
- [31] Pisana S, Lazzeri M, Casiraghi C, Novoselov K S, Geim A K, Ferrari A C and Mauri F 2007 Breakdown of the adiabatic Born–Oppenheimer approximation in graphene *Nature Mater.* **6** 198
- [32] Stampfer C, Molitor F, Graf D, Ensslin K, Jungen A, Hierold C and Wirtz L 2007 Raman imaging of doping domains in graphene on SiO₂ *Appl. Phys. Lett.* **91** 241907
- [33] Yan J, Zhang Y, Kim P and Pinczuk A 2007 Electric field effect tuning of electron–phonon coupling in graphene *Phys. Rev. Lett.* **98** 166802
- [34] Nonnenmacher M, O’Boyle M P and Wickramasinghe H K 1991 Kelvin probe force microscopy *Appl. Phys. Lett.* **58** 2921
- [35] Jacobs H O, Knapp H F, Müller S and Stemmer A 1997 Surface potential mapping: a qualitative material contrast in SPM *Ultramicroscopy* **69** 39
- [36] Filleter T, Emtsev K V, Seyller Th and Bennewitz R 2008 Local work function measurements of epitaxial graphene *Appl. Phys. Lett.* **93** 133117
- [37] Ziegler D, Gava P, Güttinger J, Molitor F, Wirtz L, Lazzeri M, Saitta A, Stemmer A, Mauri F and Stampfer C 2011 Variations in the work function of doped single- and few-layer graphene assessed by Kelvin probe force microscopy and density functional theory *Phys. Rev. B* **83** 235434
- [38] Ooi N, Rairkar A and Adams J 2006 Density functional study of graphite bulk and surface properties *Carbon* **44** 231
- [39] Sque S J, Jones R and Briddon P R 2007 The transfer doping of graphite and graphene *Phys. Status Solidi a* **204** 3078
- [40] Giovannetti G, Khomyakov P, Brocks G, Karpan V, van den Brink J and Kelly P 2008 Doping graphene with metal contacts *Phys. Rev. Lett.* **101** 026803
- [41] Yu Y-J, Zhao Y, Ryu S, Brus L E, Kim K S and Kim P 2009 Tuning the graphene work function by electric field effect *Nano Lett.* **9** 3430
- [42] Wang R, Wang S, Zhang D, Li Z, Fang Y and Qiu X 2011 Control of carrier type and density in exfoliated graphene by interface engineering *ACS Nano* **5** 408
- [43] Sabio J, Seoáñez C, Fratini S, Guinea F, Neto A and Sols F 2008 Electrostatic interactions between graphene layers and their environment *Phys. Rev. B* **77** 195409